THE CURLOMETER AND OTHER GRADIENT MEASUREMENTS WITH CLUSTER

M. W. Dunlop[1,2], A. Balogh[2], Q-Q. Shi[3], Z. Pu[4], C. Vallat[5], P. Robert[6], S. Haaland[7], C. Shen[3], J. A. Davies[1], K.-H. Glassmeier[8], P. Cargill[2], F. Darrouzet[9], A. Roux[6].

[1]*SSTD, Rutherford Appleton laboratory, Chilton, Didcot, Oxon, OX11 0QX, UK, Email: m.w.dunlop@rl.ac.uk*
[2]*Imperial College, Exhibition Road, London SW7 2BW, UK*
[3]*Centre for Space Science and Applied Research, Chinese Academy of Sciences, Beijing 100080, China*
[4]*School of Earth and Space Sciences, Peking University, Beijing 100871, China*
[5]*Centre d'Etude Spatiale des Rayonnements, Toulouse Cedex 4, France*
[6]*Centre d'Etude des Environnements Terrestre et Planetaires/IPSL, Velizy, France*
[7]*Max-Planck-Institut fuer extraterrestrische Physik, P.O. Box 1312, 85741, Garching, Germany.*
[8]*Institut für Geophysik und extraterrestrische Physik, Technische Universität Braunschweig, Mendelssohnstrasse 3, D-38106 Braunschweig, Germany*
[9]*Belgian Institute for Space Aeronomy (IASB-BIRA), Avenue Circulaire, 3, B- 1180 Brussels, Belgium*

ABSTRACT

The four-spacecraft, magnetic field measurements on Cluster can produce an accurate determination of the electric current point by point in time (the Curlometer technique). For example, for planar events, the thickness of the current layer can be accurately estimated from its magnetic profile at each spacecraft and the corresponding boundary crossing times. The latter give a determination of boundary motion relative to the Cluster array. For a range of spacecraft separation distances, the estimate of electric current density can be representative even when the configuration of Cluster spacecraft approaches the thickness of the current layer. The magnitude of the current is often accurately represented and in principle can be tracked through any structure. Minimum variance analysis on the curlometer measurements can be used to estimate the normal to a current layer. Other methods exist which are based on estimation of the magnetic gradients, curvature, or temporal derivative. These methods can be used to calculate a number of other properties, such as the dimensionality of the structure and the corresponding velocity, the field curvature, or boundary normals, but have the commonality of providing a quantity at every moment in time, like the curlometer.

1. INTRODUCTION

Until the advent of the four spacecraft Cluster mission [*Space science reviews, 1997*], direct measurement of spatial gradients, and the vector current density in particular, have not been possible. In the case of boundary layers, the spatial array of Cluster spacecraft also allows the local geometry and spatial extent to be determined so that the multi-point data allows a direct comparison of the current within the boundary layer as it is traversed. The four Cluster spacecraft were launched in pairs on two Soyuz rockets on the 16th July and the 9th August 2000 and were placed into eccentric (4 R_E x 19.6 R_E), inertial, polar orbits. Throughout a year, the orbit covers the dayside magnetopause at high latitude near local noon and low latitude near the dawn and dusk flanks. The spacecraft fly in an evolving configuration, which repeats every orbit (apart from minor perturbations), but which has been changed at intervals during the mission to cover a large range of spacecraft separation distances (100-6000 *km*) at the magnetopause. The results presented here therefore have been confirmed over a variety of spatial scales.

The magnetopause boundary, for example, has been extensively studied for many years [e.g. 1,2,3,4,5,6]. Previous multi-point observations of the magnetopause layer, however, have primarily arisen only from dual spacecraft: ISEE1 and 2 [7,8] and AMPTE IRM and UKS [9] measurements [e.g. 10,11,12], although estimates of the current density have been attempted in the past [e.g. 13]. Individual spacecraft crossing the magnetopause sample changes in the magnetic field across the current layer, which, in a 1-D geometry, can in principle give an estimate of the current magnitude in the boundary. These estimates, however, depend on accurate knowledge of the orientation and motion of the boundary, in order to obtain positions within the layer. A number of single spacecraft techniques exist to estimate boundary orientation and motion, but the four-spacecraft Cluster magnetic field measurements [14], used alone, have allowed direct determination of the boundary motion, giving accurate measurement of the boundary thickness and orientation [15]. The local current density [16] can also be estimated from the four spacecraft magnetic field measurements alone and we directly compare these quantities for a number of events covering

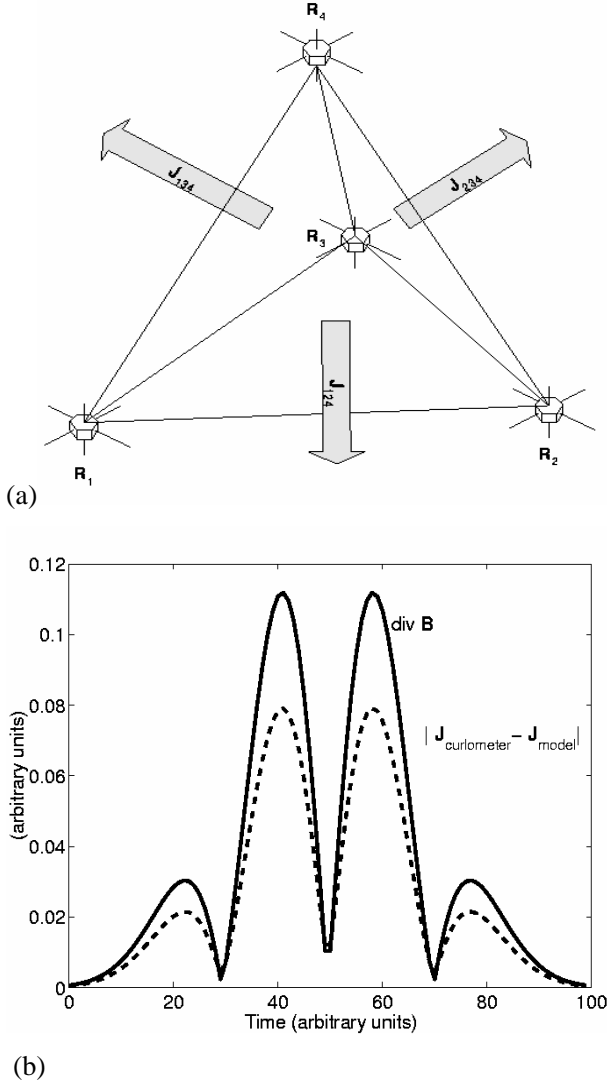different spatial scales and different geometrical circumstances.

(a)

(b)

Figure 1: (a) Summary of the curlometer calculation (see also [17,18]), (b) Sample comparison between the error in the linear curlometer estimate and the linear estimate of div(B) for a simple current sheet.

A number of related four spacecraft techniques now exist [e.g. 19,20,21], some making either a variety of assumptions or using other measurements. The magnetic field measurements, however, have proved to be a key dataset to unlock the Cluster multi-point measurements: they have provided accurate quantities at each point in time and provide a particular context for plasma measurements. The multi-spacecraft analysis of events, however, depends upon the temporal behaviour, and most methods assume some degree of stationarity in the interpretation. A key intention of this report is to show how robust the basic methods are (rather than presenting comparative analysis of the four spacecraft data), with the virtue of using only one type of measurement having extremely high accuracy, namely the magnetic field, which is supported by the high accuracy of the auxiliary position data.

In addition to the magnetopause current layer, we review the application of the curlometer to a number of other magnetic structures, such as FTEs, the cusp boundaries, the magnetotail and the ring current. A characteristic of the curlometer analysis is that the current is estimated point by point in the time series data, and this is a general feature of most gradient-based analysis. We also briefly review the application of a number of these other techniques.

2. BASIC CURLOMETER METHOD

The fluxgate magnetometer (FGM) experiment provides high time resolution magnetic field measurements on all four Cluster spacecraft [14] at 22.4 Hz (normal mode) or 67 Hz (burst mode). The instruments are operating continuously and the data have been filtered and re-sampled onboard from an internal sampling rate of 202 Hz. The data are believed to be inter-calibrated to at least 0.1 nT accuracy overall. Here, we employ both spin resolution and high time resolution data where appropriate, which has been re-calibrated to higher accuracy where necessary. The time series data shown in the plots is at spin resolution.

The discontinuity analyser (DA) technique determines parameters that describe the motion, geometry and orientation of discontinuities. The basic algorithm determines boundary normals at each spacecraft crossing point independently (using Minimum Variance Analysis [22], for example). It is applied here in the case of stationary, planar boundaries, where the normals are all found to be parallel. The boundary orientation and motion can then be calculated by combining the boundary crossing times with the spacecraft separation vectors. Because the normals are determined independently, parallel normals not only imply a planar geometry over the spacecraft array, but provide mutual confirmation of the boundary orientation (mean normal), which then allows the boundary motion (v_n, a_n), to be determined from

$$r_n = v^0_n t + \tfrac{1}{2} a_n t^2 \qquad (1)$$

where $r_n = \Delta r_{ij} \cdot \mathbf{n}$, $t = t_{ij}$, etc. and i,j refer to the spacecraft.
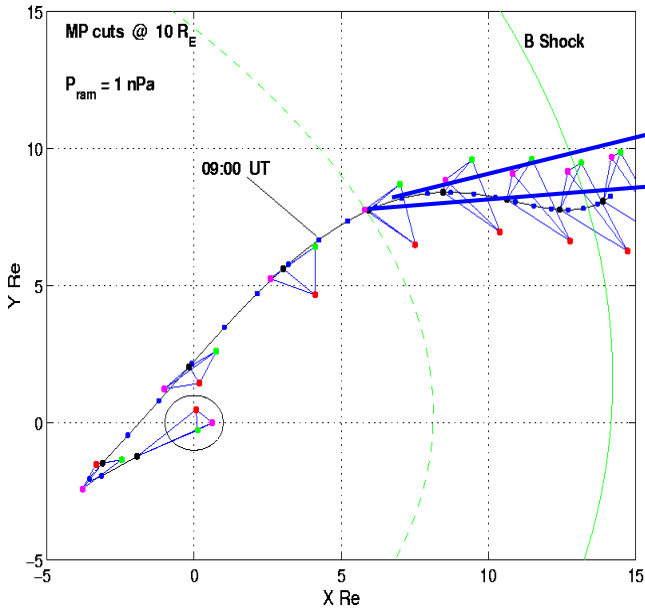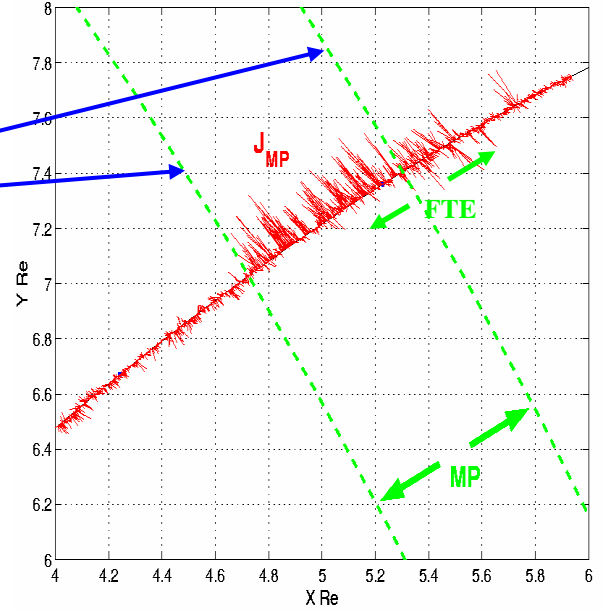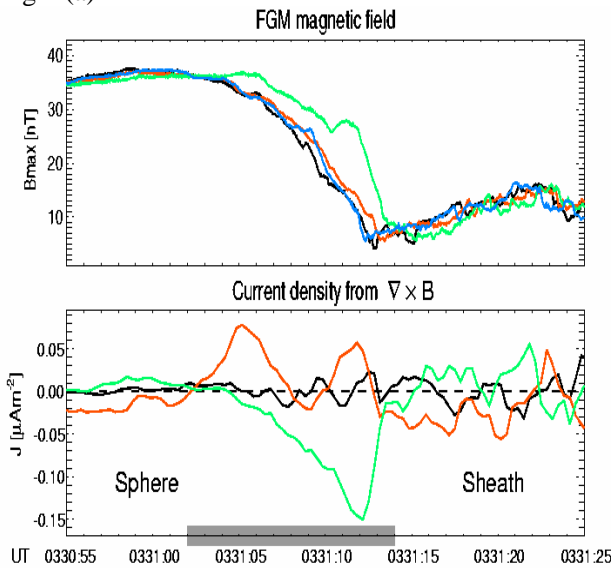
Fig 2 (a)

Fig2 (b)

Fig2 (c)

Figure 2: The analysis of the 26th January 2001. (a) The Cluster orbit track, projected into the GSM X,Y plane, together with the configuration of the four spacecraft, enlarged by a factor of 20 at intervals along the orbit. Magnetopause and bow shock curves are shown at the high of the orbit track and for the observed solar wind pressure, as indicated. (b) The computed current estimate from the curlometer, projected into the plane along the orbit track (given in nAm^{-2}, scaled down by a factor of 10). The dashed lines indicate the extreme positions on the orbit within which the magnetopause is encountered. The magnetopause moves inward and outward several times during the interval, resulting in the bursts of current which are apparent from the projections. (c) The current density calculation for a thin current sheet (~100 km) on the 2nd March 2002.

If the motion is constant (a_n approximately zero), equation 1 can be used to compute $\mathbf{n}/v_n^0$ [after 23]. The computation of $\mathbf{n}$ and v_n^0, made by assuming constant velocity, is referred to as a timing analysis, since it only depends on the timing of the crossings at each spacecraft. In practice, application requires

identifiable, stationary features in the time series data, usually best viewed in the maximum variance component of the magnetic field. For the case of well-defined current sheets, this component will suggest a magnetic field rotation over some finite time interval (traversal time to cross the current

sheet). Once any change in velocity has been found, each traversal time through the current layer can be scaled to a boundary thickness (at each spacecraft).

The first application of the curlometer technique to Cluster data has been reported by [16]. As shown in Figure 1(a), the method combines simultaneous, vector magnetic field data from each spacecraft with the spacecraft positions to calculate the curl of the magnetic field from Ampère's law (giving an estimate of the average current density through the spacecraft configuration), using the difference approximation

$$\mu_0 \boldsymbol{J} \cdot (\Delta \boldsymbol{r}_i \wedge \Delta \boldsymbol{r}_j) = \Delta \boldsymbol{B}_i \cdot \Delta \boldsymbol{r}_j - \Delta \boldsymbol{B}_j \cdot \Delta \boldsymbol{r}_i$$
$$\left\{ \text{representing} : \ \mu_0 \int \boldsymbol{J} \cdot ds = \oint \boldsymbol{B} \cdot dl \right\}$$

with $\Delta \boldsymbol{r}_i \equiv \boldsymbol{r}_i - \boldsymbol{r}_1$, and similarly $\Delta \boldsymbol{B}_i \equiv \boldsymbol{B}_i - \boldsymbol{B}_1$, giving the average current normal to each face (1,i,j) of the spacecraft tetrahedron. Since each face is known by $\Delta \boldsymbol{r}_i \wedge \Delta \boldsymbol{r}_j$, the currents normal to three faces can be re-projected into a Cartesian co-ordinate system. It is also possible to calculate an estimate for $div(\boldsymbol{B})$, from

$$div(\boldsymbol{B}) | \ \Delta \boldsymbol{r}_i \cdot \Delta \boldsymbol{r}_j \wedge \Delta \boldsymbol{r}_k | = | \Sigma_{cyclic} \Delta \boldsymbol{B}_i \cdot \Delta \boldsymbol{r}_j \wedge \Delta \boldsymbol{r}_k |,$$

which produces non zero values, partially as a consequence of non-linear spatial gradients neglected in its estimate. This quantity therefore usefully measures an effect of the linear approximation and we use it as a monitor of this error. Figure 1(b) shows an illustration of the comparison between the estimate of div(B) and the actual error in the approximation for a simple current sheet model. For other, more complex, structures and for non regular configurations, div(B) is often less useful as an estimator.

3. MAGNETOPAUSE ANALYSIS

3.1 Establishing the MP current

We first demonstrate that the curlometer technique is able to consistently estimate the magnetopause current using an example taken from 26th January 2001. The top left-hand panel in Figure 2 shows the spacecraft configurations (enlarged by a factor of 20) along the orbit which correspond to an outbound pass through the dayside magnetopause, crossing at high ($\sim$9.5 R_E) latitude on the dusk-side of the cusp, as shown. In this Figure (and the others showing the orbit track) the dots along the orbit are at hour intervals. The mean spacecraft separation distance was 600 km. These data have been reported by [24,25,26] and exhibit a key interval of repeated boundary layer crossings as a result of inward and outward motion of the magnetopause between 10 and

11 UT (which has a mean thickness of $\sim$1200 km and mean speed of $\sim$25 km/s).
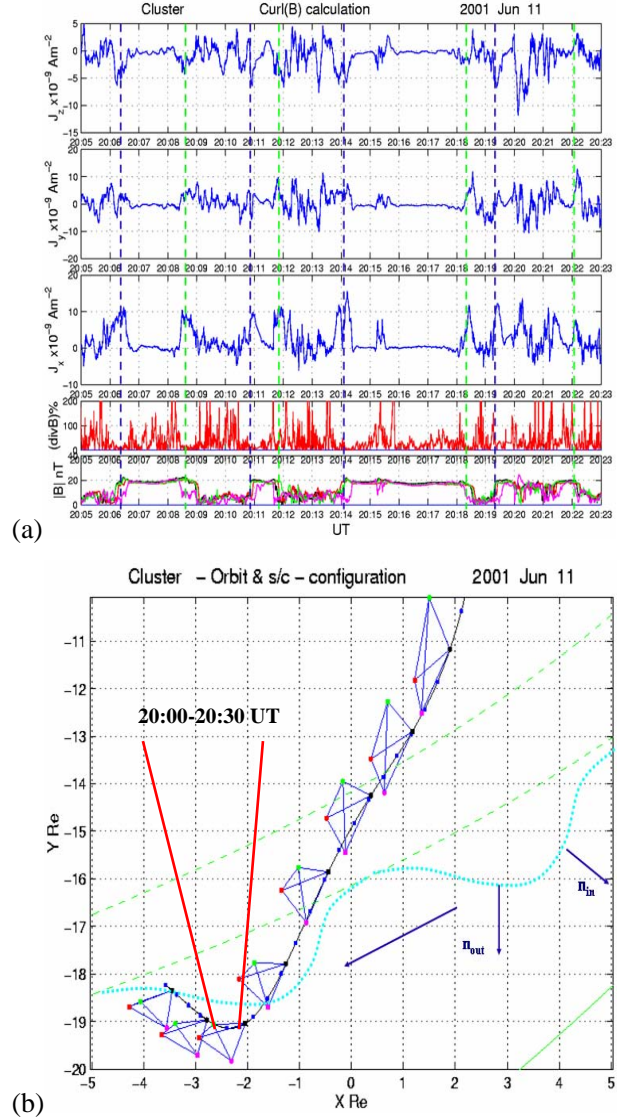

(a)

(b)

Figure 3: The analysis of the 11th June 2001, showing (a) a plot of the curlometer estimate of GSM components of the current (top three panels), the estimate of div(B) and the total magnetic field from all four spacecraft to show the pairs of crossings to and from the magnetosphere, and (b) the orbit track and spacecraft configuration projected into GSM together with a schematic of the boundary ripples implied from the DA analysis.

The right hand plot of Figure 2 shows a short segment of the orbit, projected into X,Y_{GSM}, with cuts through the model magnetopause [27], which is placed at 10 and 11 UT so as to represent the approximate range of positions along the orbit at which the boundary is sampled. The X,Y_{GSM} components of the estimated current density are plotted along the orbit (in nAm^{-2}, scaled down by a

factor of 10) and show enhanced values within this interval and a clear alignment to the magnetopause orientation. Between 10 and 11 UT the current bursts correspond to repeated encounters with the magnetopause boundary layer, and are directed predominantly in the direction, consistent with a Chapman/Ferraro current. The mean current for this interval is: $(-7.4, 8.4, -0.65)_{GSM}$, nAm^{-2}. The overall variance in this mean current direction for all the crossings is ~14 *deg*. When the variation of the current vector is calculated only over the period of each crossing for which the magnitude is more than 60% of the peak current the vectors are aligned to within 5 *deg*.
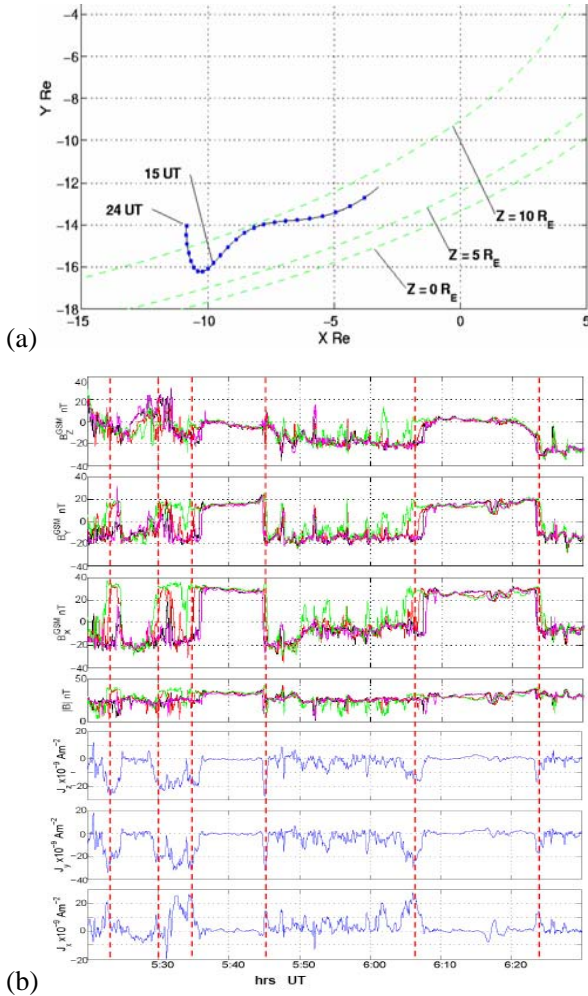

(a)

(b)

Figure 4: The analysis of the 5th July 2001. (a) The orbit track projected into GSM for the whole day, together with cuts through the magnetopause at the heights and solar wind pressure indicated. (b) A plot of the four spacecraft magnetic field data (top four panels) and GSM components of the current estimate (lower three panels), for a short interval containing a few of the magnetopause crossings observed on this day.

More detailed analysis of the individual crossings (not included here for this event, but see below for other passes) shows that the slight tilting of the current directions from crossing to crossing is consistent with corresponding tilting of the local magnetopause direction, which then accounts for the size of the variance calculated above. In contrast, enhanced values of current after 11 UT, correspond to a train of FTE (flux transfer event) signatures, associated with the occurrence of extensive reconnection during the event [26] and exhibit a variety of orientations. The mean current for this later interval is: $(0.06, -0.07, -0.9)_{GSM}$, nAm^{-2}, which is an order of magnitude lower and directed along Z_{GSM} (the mean flux tube direction), rather than the plane of the magnetopause. Figure 2c shows the estimate of the current density, with respect to minimum variance co-ordinates, through one thin current layer, for small spacecraft separation distances (~100 km). At these small spacecraft separations it is often possible to estimate the profile of current density through the layer [28 and see *Haaland et al., this issue*]: the main current signature is in the maximum variance component within the layer, whereas the peak at the edge of the layer lies in the intermediate variance component. Both are in the magnetopause plane.

3.2 Orientation to MP ripples

Figure 3 shows a second event, which occurred as the spacecraft were at apogee in the dawn flank magnetosheath, near the equatorial plane. Figure 3b shows a schematic of the boundary motion, superimposed onto the orbit which is shown projected into the X,Y_{GSM} plane and in the same format as Figure 2. In this case the spacecraft configurations have been scaled by a factor of 5 and the mean separation distance is ~2000 *km*. The DA analysis suggests that a series of surface ripples on the magnetopause move tailward past the spacecraft array in the manner indicated, taking them fully into the magnetosphere on each occasion. The lower panel in Figure 3a shows the multi-spacecraft, magnetic field magnitude where the transitions from a quiet, 20 *nT* magnetospheric field to a low, fluctuating magnetosheath field are marked by the dashed lines.

The magnetopause orientations fall into pairs for inward/outward crossings, represented by the green and blue vertical dashed lines on the plot in Figure 3a, respectively, and match the two distinct boundary orientations shown in Figure 3b. The boundary normals are depicted by the blue arrows shown in Figure 3b (which represent their mean orientations)

and have small Z_{GSM} components. The crossings are irregular and show a different velocity projection, at each spacecraft, along the boundary normals for the crossings. This motion together with transit times through each current layer encounter (measured from the turning in the maximum variance component of the field) can be used to estimate boundary thickness (see below in Table 1), but represents a projected tailward motion along the magnetopause for each crossing. The value of divB is also included in Figure 3a to show that the value is low (~15%) at each crossing.

The other panels in Figure 3b from bottom to top show respectively the estimate of div(B) and the GSM components of curl(B), $J_{X,Y,Z}$. The value of divB is also included to show that the value is low (~15%) at each crossing. Although the spacecraft separation distances are slightly larger than the estimates of boundary thickness (see Table 1), it appears that the current density is still adequately sampled through each crossing to confirm its direction. In fact, the direction of the current maintains its alignment to the magnetopause orientation which tilts from crossing to crossing. This can be seen from the components of curl(B), which change from crossing to crossing. The J_X component is maintained for the majority of crossings, whereas the J_Y component changes such that the majority of the inward crossings (green dashed lines, taking the spacecraft back into the magnetosheath) have larger values than the outward crossings, which tend to have small J_Y components. This follows the orientations indicated for the geometry of the ripples (as shown by the arrows in Figure 3a). The J_Z component is less significant for magnetopause alignment since the normals lie nearly in the X,Y_{GSM} plane. Thus, even for this event, where the magnetopause current layer is poorly matched in scale to the spacecraft separation, the curlometer is giving a good estimate of direction.

3.3 Scaling of the current density

Figure 4 shows a further series of magnetopause crossings from a third event, on the 5th July 2001. The Cluster orbit skirted the dawn flank magnetopause during this day, maintaining a position relative to the boundary, which moved from high to low-latitudes (as shown in Figure 4a). This location provided a number of magnetopause crossings for a large fraction of the day and the interval shown in Figure 4b represents a few crossings from this set. The Figure shows the magnetic field in the top four panels and the curlometer estimate in the bottom three, all in GSM.

Distinct from the previous event and given the spacecraft separations and estimated motion determined from the DA technique, these crossings represent small amplitude (<1 R_E), inward and outward motions of the magnetopause, providing a sequence of crossings with almost parallel orientations. The bursts of current in the lower three panels reflect this common orientation by maintaining a common direction, aligned to the magnetopause plane. It should be noted however, that in this event the scale size of the boundary layer is smaller compared to the cluster separation distance (see below) and we expect a less close quantitative comparison between the current magnitude and direction. The current signature shows both slow crossings, where the spacecraft array remains in the current layer for longer so that the enhanced value of curl(B) remains for several minutes, and fast crossings, where the curl(B) profile shows a short spike.
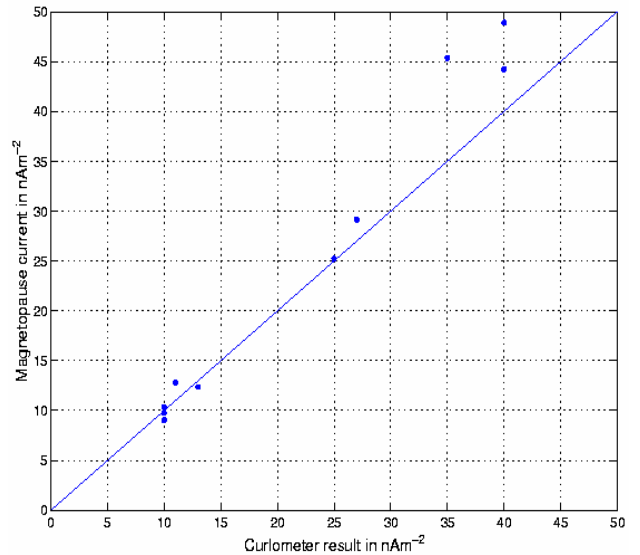

Figure 5: A scatter plot of the results in the table, showing the estimated magnetopause current (ΔB/ΔD) against the curlometer calculation (J).

These slow and fast crossings are listed in Table 1, as indicated by their mean velocities. Table 1, quantifies the results and summarises both the 11th June 2001 event and a selected set of crossings from 5th July 2001. These crossings have been analysed in detail and shows the estimated thickness of the current layer for each crossing, together with the current density estimates. The columns show respectively the event times and the crossing label (referring to 'in' and 'out' for the dashed lines in Figure 3 and to 'mp' for the dashed lines in Figure 4). From left to right the remaining columns show: the mean MVA normal and velocity (in *km/s*) from the DA technique; the corresponding timing normal and velocity (in

km/s); the average current across the current layer, estimated from the curlometer (in *nA/m²*); the change in the maximum variance component of the magnetic field across the magnetopause (in *nT*), and the estimated thickness of the current layer at each spacecraft from the DA technique (in *km*). The timing normals, shown for comparison, assume constant velocity, which is often not true for these crossings. Consequently, they highlight the sensitivity in the DA analysis to compute boundary motions, and therefore the scaling of the current thicknesses. These estimates, however, show good stability for all the crossings shown.

The results confirm that the thickness of the current layer is effectively constant while being sampled by the spacecraft array, the small variations being within the estimated errors. This thickness can be used to compute an average current density in the magnetopause from $\Delta B/\Delta D$, where ΔB and ΔD are taken from Table 1. This can then be compared to $\mu_0|J|$. For each crossing, the variation of the current follows this ratio within 15% uncertainty (worst case).

Moreover, the estimate of the current vector lies nearly perpendicular to the DA-normals also shown in the table and therefore lie parallel to the magnetopause boundary, to within the same uncertainty. The tilting of the boundary ripples in the first event, in particular, can also be seen in both the current vector and the DA normals. We do not expect such close quantitative agreement in the case of the second event where the relative scale size of the boundary is smaller (thinner), but although the errors appear to be larger, there is evidence that the scaling of the curlometer current follows that of $\Delta B/\Delta D$ as before.

These quantitative results can be read off the profiles observed in Figure 4 in particular, where the ΔB clearly changes from crossing to crossing, reflecting mainly the changing ΔD. The mean currents for each of the crossings indicated by the dashed lines are given in Table 1. The variance in these currents is <30 *deg*, reflecting the less accurate calculation of the curlometer in this case. Figure 5 shows a scatter plot of the results given in Table 1, and compares the two estimates of current from the curlometer and $\Delta B/\Delta D$ (magnetopause current), with appropriate scaling for the thickness estimates. The values of magnetopause current for the higher current values can be seen to be slightly over estimated.
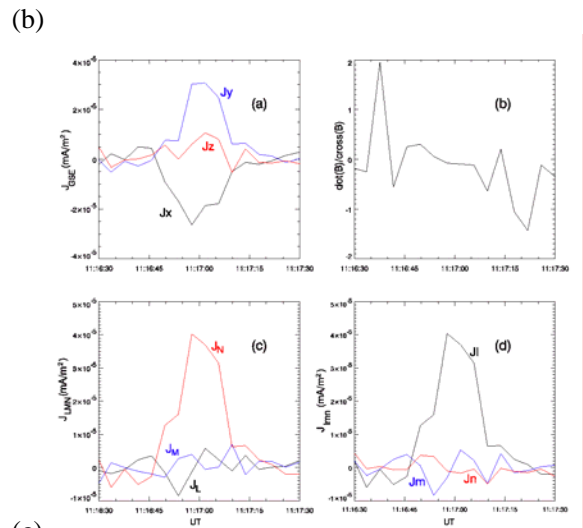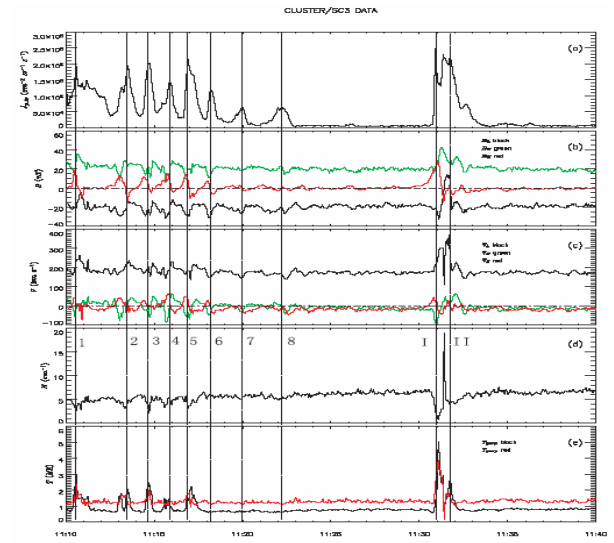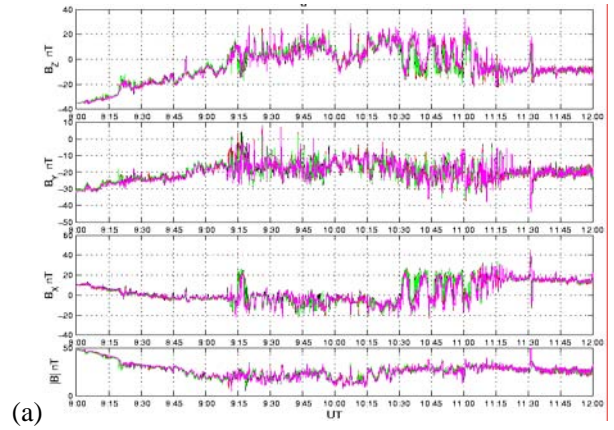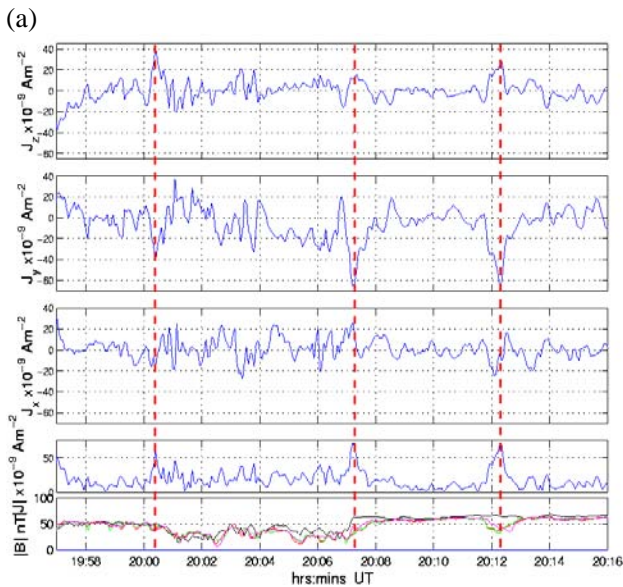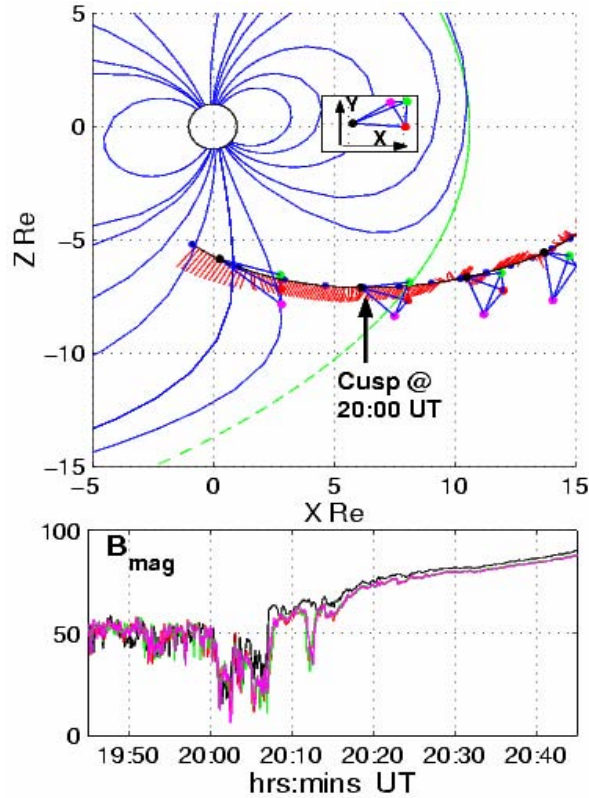

(a)

(b)

(c)

Figure 6: The magnetopause traversal on the 26 January 2001, also shown in Figure 2, showing (a) the multi-point magnetic field data for the pass, (b) the overview of the magnetosheath FTE signatures and (c) the low resolution current structure in one FTE in both GSE and minimum variance coordinates, showing the alignment to the flux tube axis.

(a)

(b)

Figure 7: Identification of the current layer at the inner and outer cusp boundaries for a cusp entry on the 13 February 2001: (a) Orbit configuration, (b) curlometer analysis.

4.   CURLOMETER FOR OTHER STRUCTURES

4.1   FTE currents

The event already shown in the previous section, 26 January 2001, also contained a large number of FTE signatures associated with a period of ongoing reconnection during the pass. The event has been analysed by several workers [e.g. 26,25,29 and *Robert et al., this issue*]. Figure 6a shows the multi-point magnetic field data for the whole pass, including a large scale FTE in the magnetosheath at 11:32 UT. Figure 6b shows this FTE and the earlier train of FTE signatures, all occurring between 11:10 and 11:40 UT, together with the energetic particle signatures. Each FTE, identified by its bipolar signature in the B_N component, contains an axially aligned current signature and an enhanced flux of out-flowing energetic ions. The axis of the implied flux tubes can be found either by MVA analysis of the FTE signature, or by minimisation of the current density [28,29], employing the condition that div(curl(B))=0, and the four spacecraft timing information (or other methods) can estimate the motion of each FTE. All these FTEs are consistent with northward moving flux tubes, connected to the northern cusp, with similar alignments. Figure 6c shows the low resolution current signature for one of these FTEs, in both GSE and MVA coordinates.

The analysis shows that the main current within the FTE is flowing along the axis of the inferred flux tube. The two lower panels show that both MVA and the minimisation of the current produced similar estimates of the true flux tube axis. The large FTE at 11:32 UT has been studied in detail by *Robert et al., [this issue]*, at high time resolution and the current profile obtained suggests that the main current lies at the edge of the flux tube and is consistent with a force free current structure, which is modelled with a double tubular cross-section.

4.2   Cusp currents

Figure 7 shows and example of the current signatures seen at both the inner and outer cusp boundaries [30]. Figure 7a shows the orbit configuration and multi-spacecraft magnetic field magnitude for the cusp entry and Figure 7b shows the corresponding bursts of current estimated by the curlometer. The outer boundary between the magnetosheath and the low field region of the cusp, at 20:00 UT, exhibits properties similar to those appropriate for a rotational discontinuity and is associated with a corresponding ion jet, consistent with that expected for a reconnection layer geometry. The inner boundary at 20:07 UT also shows that a significant current layer exists between the cusp and the lobe region of the magnetosphere. A partial encounter at 20:12 UT also contains a similar current signature.
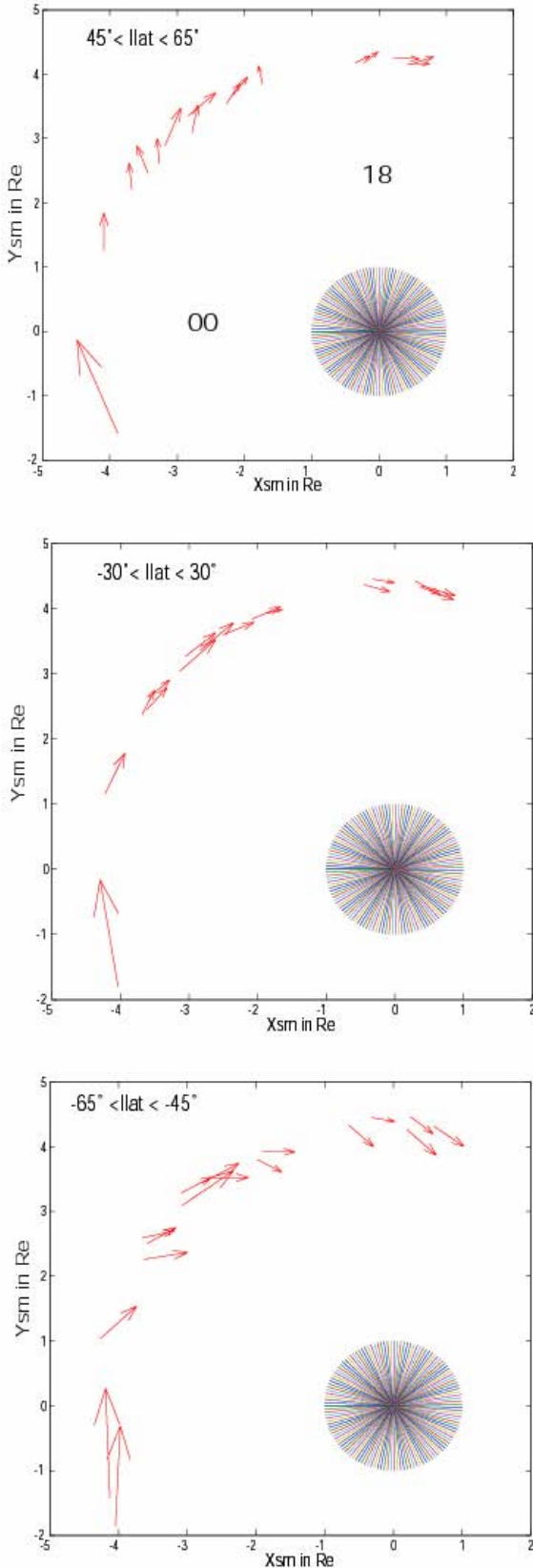
Figure 8: The confirmation of the westward ring current for a set of perigee passes covering a range of local time and latitude.

Figure 9: An example of the curlometer signature associated with the magnetotail current sheet.

4.3 The ring current

The properties of the magnetospheric ring current have also been monitored using the curlometer technique [31]. These results show that an azimuthal (westward) current is maintained at the equator which evolves into a field aligned current at the plasma sheet boundary. The signatures are limited by the spacecraft configuration, but give good estimates for the current components perpendicular to the background field. A statistical study has also been performed and this gives a clear confirmation of the ring current extending over different latitudes, as indicated by Figure 8.

4.4 The magnetotail

The curlometer has also been extensively applied to the magnetotail current sheet (see other reports in this issue) and an example of one signature is shown in

Figure 9 which occurred during an active period of current disruption associated with a near earth neutral line formation on the 11th August 2002. This signature correlates with the energetic electron signatures observed during the crossings into the current sheet (top panels of Figure 9, which show the omni-directional flux and pitch angle distributions, normalised to the peak intensity in the lower panel). These energetic electrons show trapped (90°) populations in the central current sheet and field aligned distributions at the edges of the current sheet, which is interpreted as being the edge of the reconnection layer. The curlometer reproduces the cross-tail current (mainly in the J_Y component) and also suggests the existence of field-aligned currents (J_X and J_z components), correlating with the field aligned electron populations.

5. OTHER GRADIENT ANALYSIS

One important feature of the curlometer analysis is that it provides an estimate point by point in time and therefore accesses the temporal evolution of the current structure. If the properties of the data are stationary in the sense that this observed time dependence represents a convective evolution relative to the spacecraft, the spatial form of the current structure is well resolved by the observations. The curlometer measurement, however, represents the combination of spatial gradients across the four spacecraft (to provide an average of the electric current density). Individual spacecraft have different locations within the current structure so that the interpretation of this average depends upon the temporal nature as much as on the relative spatial extent. Linear estimates of the spatial gradients can be combined into a variety of other quantities which can form other gradient based methods which are also dependent on the temporal interpretation. Some recent analysis techniques are highlight in this section.

In the general form of these methods the spatial gradient tensor can be used to find the rotation and curvature properties of the magnetic field [32], as well as the gradients in magnetic pressure. Gradient analysis has also been applied to other quantities such as the plasma density [33]. We illustrate here a simple related method, however, called the Minimum Directional Derivative method (MDD) [20], which is based on a principle value decomposition (diagonalisation) of the symmetric matrix,

$L=(\nabla B)(\nabla B)^T$, where ∇B is the dyadic of the magnetic field vector B. The analysis returns the maximum, intermediate and minimum eigenvalues and eigenvectors, $\lambda_1 n_1$, $\lambda_2 n_2$, $\lambda_3 n_3$ and the separation of the eigenvalues defines the dimensionality of the structure. For example, when the maximum eigenvalue is large compared to the others, the structure is a 1-D boundary. In addition, the convective equation, $DB/Dt+V_{str}\cdot\nabla B=0$, can directly provide an estimate of the velocity of a spatial structure, V_{str} and this can be combined with the MDD method to provide the velocity of 3-D, 2-D and 1-D (boundary layer) structures. Figure 10 shows and example of this analysis for the thin magnetopause crossing on the 2 March 2002, as shown in Figure 2c. When all the spacecraft enter the boundary, as indicated by the box, λ_1 is well separated from the others and then the corresponding eigenvector, n_1 is the boundary normal. This normal and the velocity along this normal (bottom panel) agrees well with estimates from other boundary analysis [28].
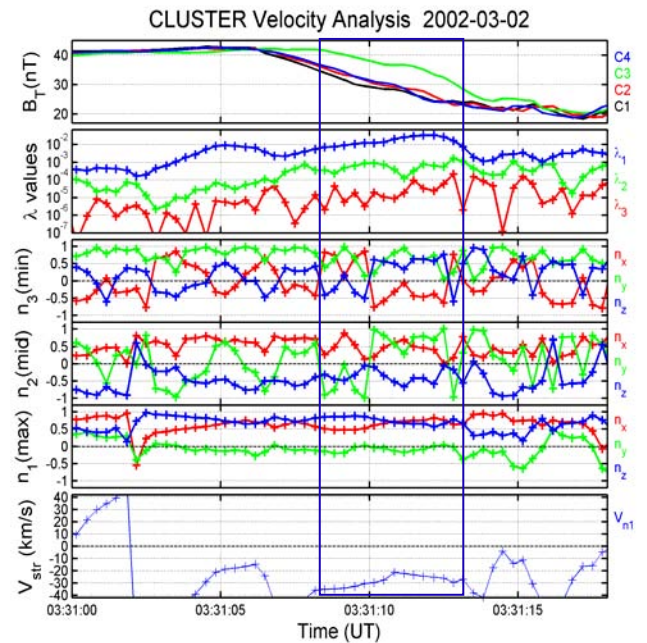

Figure 10: An example of the application of the gradient based dimensionality and motional analysis for the magnetopause crossing shown in Figure 2c. The top panel shows the magnetic field profile, the second panel shows the eigenvalues, the next three panels show the corresponding eigenvectors and the bottom panel shows the velocity along the normal to this 1-D structure.

Table 1: Summary of the boundary analysis for crossings from two days, giving the boundary normals (n) and speed from both the DA and timing analysis, the curlometer (current in nAm^{-2}) and the thickness (ΔD in km) for each event. Magnetic field is given in nT and velocities in km/s. The boundary normals are unit vectors.

Date	UT	MP	λ_2/λ_3	$<n_{GSE}>$			$<V_n>$	n_{timing}			V_{timing}	J_{GS}			$|J|$	ΔB	ΔD_1	ΔD_2	ΔD_3	ΔD_4
11/06/2001	20:06:30	1-out	15.3	0.27	-0.94	0.19	120	0.03	-0.83	0.56	61	8	3	-4	10	18	1214	1244	1214	1171
		1-in	9.0	0.70	-0.62	-0.36	-104	0.22	-0.95	0.22	-45	8	6	-2	10	19	1297	1380	1331	1438
	20:11:00	2-out	5.0	0.46	-0.88	0.13	155	-0.16	-0.82	0.55	106	8	3	-4	10	19	1514	1492	1420	1448
		2-in	5.7	0.66	-0.73	0.21	-74	0.68	-0.48	0.55	-106	9	7	-4	11	23	1088	1031	1154	1120
	20:14:00	3-out	7.7	0.07	-0.99	0.15	32	0.34	-0.94	0.04	71	11	4	-5	13	25	1228	1545	1412	1358
		3-in	4.8	0.79	-0.61	-0.10	-165	0.43	-0.88	0.19	-97	8	7	-2	10	17	1002	1008	1029	1030
05/07/2001	05:24:00	mp	11.0	0.53	-0.84	-0.11	-111	0.41	-0.81	-0.41	-89	5	-20	-15	27	59	751	595	551	710
	05:35:00	mp	3.0	0.36	-0.84	0.41	20	0.43	-0.87	0.25	17	24	-26	-18	40	55	274	291	299	318
	05:45:00	mp	6.0	0.64	-0.76	-0.11	-22	0.53	-0.82	0.19	-44	14	-30	-25	40	63	450	391	415	481
	06:06:00	mp	7.8	0.28	-0.85	0.44	11	0.24	-0.82	0.52	11	22	-22	-15	35	51	344	356	367	350
	06:23:00	mp	3.7	0.61	-0.78	-0.03	-23	0.54	-0.83	0.17	-41	13	-17	-16	25	53	836	761	761	867

6. CONCLUSIONS

We have shown that the magnetic field measurements on Cluster can produce a realistic determination of the electric current density at the magnetopause, even where the scale size of the Cluster configuration approaches that of the current layer thickness, using a series of planar magnetopause crossings with significant shear. The vector current densities have been shown to lie in the plane of the magnetopause boundary (to within 15%), even during times of induced motion and large-scale surface ripples. This is the first time that in situ measurements have directly measured the magnetopause current. These results have depended upon first accurately determining the orientation and thickness of the current layer, using the four spacecraft DA technique. In combination with the curlometer estimate of curl(B), the current profiles have been shown to compare well to the mean current defined by the overall magnetic shear across the boundary layer. The thicknesses determined here, for a number of crossings from the three passes, vary between 300-1500 *km*(see Table 1), which is comparable, for each pass, to the estimated range of ion gyroradii. The corresponding current densities range from ~9 *nAm^{-2}*, for the thickest boundaries, to ~40 *nAm^{-2}*, for the thinnest. The magnetopause crossing speeds (not shown here) ranged from ~10-30 *km/s* (at the location near local noon) to ~100-150 *km/s* (at the dawn flank location).

Knowledge of the boundary orientation and motion in principle allows a mapping of time to spatial location in the current layer (through: $\delta x = v_n \delta t$, if x lies along the boundary normal). This allows the current density to be compared to the magnetic field change with distance through the layer. For example, the current estimates shown in Figures 1-3 all show simple peak-profiles though each encounter with the magnetopause. Some correspond to fast (sharp) crossings and some to slow encounters. Given the velocity estimates from the DA technique at each spacecraft (v_n), the change in the magnetic field component with time through the magnetopause can therefore be related to distance through the boundary layer, and hence to the current profile (since: $v_n \mu_0 / |J| = \delta B / \delta t$). This information is limited, of course by the relative scale size of the Cluster array and changing velocity at each spacecraft, since the curlometer gives a mean current estimate over the whole spacecraft volume. Future work is underway which explores the use of the average field over the four spacecraft in this context and using selected crossings at small spacecraft separations and constant boundary motion.

Other applications of the curlometer to: flux tubes, represented by FTEs; the magnetotail; the cusp, and the ring current, have also been reviewed briefly here. These results all indicate that a very wide application of the curlometer is possible which provides meaningful results. We have also highlighted some other recent gradient-based methods which add to the point by point analysis and give results which compare well with other methods.

REFERENCES

1. Berchem, J. and Russell, C. T., The thickness of the magnetopause current layer: ISEE 1 and 2 observations, *J. Geophys. Res.*, **87**, 2108-2114, 1982.

2. Russell, C. T., The structure of the magnetopause, *in Physics of the Magnetopause, P. Song, B.U.O. Sonnerup, M.F. Thompsen (eds)*, AGU Geophysical Monograph **90**, 81-98, 1995.

3. Paschmann, G., Papamastorakis, I., Baumjohann, W., Skopke, N., Carlson, C. W., Sonnerup, B. U. Ö. and Lühr, H., ISEE observations of the magnetopause: Reconnection and the energy balance, *J. Geophys. Res.*, **90**, 12111-12120, 1985.

4. Paschmann, G., Papamastorakis, I., Baumjohann, W., Skopke, N., Carlson, C. W., Sonnerup, B. U. Ö. and Lühr, H, The Magnetopause for large magnetic shear: AMPTE/IRM observations, *J. Geophys. Res.*, **91**, 11099-11115, 1986.

5. Phan, T. -D., Paschmann, G., Baumjohann, W., Skopke, N. and Lühr, H., The magnetosheath region adjacent to the dayside magnetopause: AMPTE/IRM observations, *J. Geophys. Res.*, **99**, 121-141, 1994.

6. Phan, T. -D. and Paschmann, G., The magnetosheath region adjacent to the dayside magnetopause, *in Physics of the Magnetopause*, *P. Song, B.U.O. Sonnerup, M.F. Thompsen (eds)*, AGU Geophysical Monograph **90**, 115-122, 1995.

7. Russell, C. T. and Elphic, R. C., Initial ISEE magnetometer results: Magnetopause observations, *Space Sci. Rev.*, **22**, 681-715, 1978.

8. Russell, C. T. and Elphic, R. C., ISEE observations of flux transfer events at the dayside magnetopause, *Geophys. Res. Lett.*, **6**, 33-36, 1979.

9. Bryant, D. A., Krimigis, S. M. and Haerendel, G. Outline of the Active Magnetospheric Particle Tracer Explorers (AMPTE) mission, *IEEE Trans. Geosci. Remote Sensing*, **GE-23**, 177-181, 1985.

10. Elphic, R. C., Multipoint observations of the magnetopause: results from ISEE and AMPTE, *Adv. Space Res.*, **8**, 223-238, 1988.

11. Elphic, R. C., Observations of flux transfer events: are FTE's flux ropes, islands, or surface waves?, *in Physics of the Magnetic Flux Ropes*, *C.T. Russell, E.R. Priest, L.C. Lee. (eds)*, AGU Geophysical Monograph **58**, 455-471, 1990.

12. Elphic, R. C., Observations of flux transfer events: a review, *in Physics of the Magnetopause*, *P. Song, B.U.O. Sonnerup, M.F. Thompsen (eds)*, AGU Geophysical Monograph **90**, 225-233, 1995.

13. Van Allen, J. A. and Adnan, J., Observed currents on the Earth's high-latitude magnetopause, *J. Geophys. Res.*, **97**, 6381-6395, 1992.

14. Balogh, A., Carr, C. M., Acuna, M. H., Dunlop, M. W., Beek, T. J., Brown, P., Fornacon, K. –H., Georgescu, E., Glassmeier, K. –H., Harris, J., Musmann, G., Oddy, T. and Schwingenschuh, K.: The Cluster magnetic field investigation: overview of in-flight performance and initial results, *Ann. Geo.*, **19**, 1207-1217, 2001.

15. Dunlop, M. W., Balogh, A., Glassmeier, K.-H. and the FGM team, Four-Point Cluster Application Of Magnetic Field Analysis Tools: The Curlometer, *J. Geophys. Res.*, **107**, 1384-1398, 2002a.

16. Dunlop, M. W., Balogh, A., Glassmeier, K.-H. and the FGM team, Four-Point Cluster Application Of Magnetic Field Analysis Tools: The Discontinuity Analyser, *J. Geophys. Res.*, **107**, 1399-1411, 2002b.

17. Dunlop M.W., Southwood D.J., Glassmeier K.-H. and Neubauer F.M., Analysis of multipoint magnetometer data, *Adv. Space Res.*, **8**, 273, 1988.

18. Robert, P., Dunlop, M.W., Roux, A., and Chanteur, G., `Accuracy of Current Density Determination', in `Analysis Methods for Multispacecraft Data', *ISSI Science Report*, **SR-001**, Kluwer Academic Pub., 1998.

19. Haaland, S. E., Sonnerup, B., Dunlop, M. W., Balogh, A., Georgescu, E., Hasegawa, H., Klecker, B., Paschmann, G., Puhl-Quinn, P., Reme, H., Vaith, H., and Vaivads, A., Four-spacecraft determination of magnetopause orientation, motion and thickness: comparison with results from single-spacecraft methods, *Ann. Geo.*, **22**, 1347-1365, 2004a.

20. Shi, Q Q, C Shen, Z Y Pu, M W Dunlop, Q.-G. Zong, H. Zhang, C. J. Xiao, Z. X. Liu and A. Balogh, Dimensional analysis of observed structures using multipoint magnetic field measurements: Application to Cluster, *Geophys. Res. Lett.*, **32**, doi:10.1029/2005GL022454, 2005.

21. Paschmann et al., Outer Magnetospheric Boundaries: Cluster Results, *Space Science Reviews*, **118**, 1-4, 2005.

22. Sonnerup, B. U. O. and Cahill, L. J., Magnetopause structure and attitude from Explorer 12 observations, *J. Geophys. Res.*, **72**, 171-183, 1967.

23. Russell, C. T., Mellott, M. M., Smith, E. J., and King, J. H., Multiple observations of interplanetary shocks: four spacecraft determination of shock normals, *J. Geophys. Res.*, **88**, 4739-4748, 1983.

24. Bosqued, J.-M., Phan, T. D., Dandouras, I., Escoubet, C. P., Rème, H., Balogh, A.,

Dunlop, M. W., Alcaydé, D., Amata, E., Bavassano-Cattaneo, M-B., Carlson, C., DiLellis, A. M., et al., Cluster Observations of the High-Latitude Magnetopause and Cusp: First Results from the CIS Ion Instruments, *Ann. Geo.*, **Cluster special issue, 19**, 1545-1566, 2001.

25. Pu, Z. Y., Zong, Q. G. , Fritz, T., Xiao, C. J., Huang, Z. Y., Fu, S. Y., Shi, Q. Q., Dunlop, M. W., Glassmeier, K.-H., Balogh, A., Daly, P., Cao, J.-B., Liu, Z.-X., Reme, H. and Dandouras, J., Multiple Flux Rope Events at the High-latitude Magnetopause: Cluster/Rapid Observation on January 26, 2001, *in press, Surveys of Geophysics*, 2005.

26. Phan, T., Dunlop, M. W., Paschmann, G, Klecker, B., Bosqued, J.-M., Reme, H., Balogh, A., Twitty, C., Mozer, F. S., Carlson, C. W., Mouikis, C. and Kistler, L. M., Cluster Observations of Continuous Reconnection at the Magnetopause under Steady Interplanetary Magnetic Field Conditions, *Ann. Geo.*, 22, 2355-2367, 2004.

27. Sibeck, D. G., Lopez, R. E. and Roelof, E. C., Solar wind control of the magnetopause shape location and motion, *J. Geophys. Res.*, **96**, 5489-5495, 1991.

28. Haaland, S, Sonnerup, BUO, Dunlop, MW, Georgescu, E, Paschmann, G, Klecker, B, Vaivads, A., Orientation and motion of a discontinuity from Cluster curlometer capability: Minimum variance of current density, *Geophys. Res. Lett.*, **31** (10), L10804, doi:10.1029/2004GL020001, 2004b.

29. Xiao, C. J., Z. Y. Pu, Z. W. Ma, S. Y. Fu, Z. Y. Huang, and Q. G. Zong, Inferring of flux rope orientation with the minimum variance analysis technique, *J. Geophys. Res.*, **109**, 11218, doi:10.1029/2004JA010594, 2004.

30. Dunlop, M.W., B. Lavraud, P. Cargill, M.G.G.T. Taylor, A. Balogh, H. Reme, P. Decreau, K.-H. Glassmeier, R.C. Elphic, J.-M. Bosqued, A.N. Fazakerley, I. Dandouras, C.P. Escoubet, H. Laakso, A. Marchaudon, Cluster Observations of the Cusp: Magnetic Structure and Dynamics, in press, *Surveys in Geophysics.*, 2005.

31. Vallat, C., I Dandouras, M Dunlop, A Balogh, E Lucek, G Parks, M Wilber, E Roelof, G Chanteur, H Rème, First current density estimate in the ring current region using simultaneous multi-spacecraft CLUSTER-FGM data, in press, *Ann Geophys.*, 2005.

32. Shen, C., X. Li, M. Dunlop, Z. X. Liu, A. Balogh, D. N. Baker, M. Hapgood, and Xinyue Wang, Analyses on the Geometrical Structure of Magnetic Field in the Current Sheet Based on Cluster Measurements, *J. Geophys. Res.*, **108**, 1168, 2003.

33. Darrouzet, F., Décréau, P., De Keyser, J., Masson, A., Gallagher, D., Santolik, O., Sandel, B., Trotignon, J., Rauch, J., Le Guirriec, E., Canu, P., Sedgemore, F., André, M., and Lemaire, J., Density structures inside the plasmasphere: Cluster observations, Ann. Geophys., **22**, 2577-2585, 2004.